Erythrocyte CD55 mediates the internalization of *Plasmodium falciparum* parasites

Bikash Shakya[1], Saurabh D. Patel[2], Yoshihiko Tani[3], and Elizabeth S. Egan[1*]

[1]Departments of Pediatrics and Microbiology & Immunology, Stanford University School of Medicine, Stanford, CA 94305, USA

[2]Zuckerman Institute, Columbia University, New York City, NY 10027, USA

[3]Japanese Red Cross Osaka Blood Center, Osaka, Japan

*Correspondence: eegan@stanford.edu

Abstract

Invasion of human erythrocytes by the malaria parasite *Plasmodium falciparum* is a multi-step process. Previously, a forward genetic screen for *P. falciparum* host factors identified erythrocyte CD55 as essential for invasion, but its specific role and how it interfaces with the other factors that mediate this complex process are unknown. Using CRISPR-Cas9 editing, antibody-based inhibition, and live cell imaging, here we show that CD55 is specifically required for parasite internalization. Pre-invasion kinetics, erythrocyte deformability, and echinocytosis were not influenced by CD55, but entry was inhibited when CD55 was blocked or absent. Visualization of parasites attached to CD55-null erythrocytes point to a role for CD55 in progression of the moving junction. Our findings demonstrate that CD55 acts after discharge of the parasite's rhoptry organelles, and plays a unique role relative to all other invasion receptors. As the requirement for

CD55 is strain-transcendent, these results suggest that CD55 or its interacting partners may hold potential as therapeutic targets for malaria.

Key Words

Malaria, CD55, erythrocyte, invasion, *Plasmodium falciparum*

Introduction

Malaria is caused by Apicomplexan parasites of the genus *Plasmodium*, of which *Plasmodium falciparum* is responsible for the majority of severe disease cases in humans. One of the world's major public health problems, malaria causes an estimated 216 million infections and ~445,000 deaths annually, primarily among young children and pregnant women (WHO, 2018). *P. falciparum* has a complex life cycle involving stages in the human and mosquito, but disease only occurs during the blood stage, when parasites infect and replicate in human red blood cells (RBCs). As *P. falciparum* is an obligate intracellular parasite, understanding the molecular determinants of its developmental cycle within RBCs may lead to new therapies. For example, a number of *Plasmodium* proteins that play key roles during erythrocyte invasion have shown promise as vaccine candidates (Ord, Rodriguez, & Lobo, 2015; Sack, Kappe, & Sather, 2017; Salinas, Tang, & Tolia, 2019). Since natural genetic variation in red cells can influence innate susceptibility to malaria, host erythrocyte factors may also hold potential as therapeutic targets (Taylor & Fairhurst, 2014). The identification and study of such factors, however, has been severely limited by the intractability of mature RBCs, which lack a nucleus and DNA.

47

48 *P. falciparum* invasion of erythrocytes involves a series of coordinated events that unfold
49 rapidly over the course of ~2 minutes. These events can be divided into three phases:
50 pre-invasion, active invasion, and echinocytosis (Gilson & Crabb, 2009; Weiss et al.,
51 2015). The process is initiated with the rupture of a "mother" parasite, termed a schizont,
52 which releases up to 32 daughter merozoites. During the pre-invasion phase, a free
53 merozoite makes initial contact with the red cell, stimulating shallow deformation of the
54 host cell plasma membrane. Next, the merozoite reorients so its apically-localized
55 organelles are abutting the cell surface. Reorientation is associated with significant
56 membrane deformation and involves interactions between *P. falciparum* ligands such as
57 the erythrocyte binding antigen (EBA) and reticulocyte binding-like homologues (Rh)
58 family proteins, and receptors on the red cell surface (Gilson & Crabb, 2009; Paul, Egan,
59 & Duraisingh, 2015; Riglar et al., 2011; Tham, Healer, & Cowman, 2012; Weiss et al.,
60 2015). Several ligand and receptor pairs have been shown to act at this stage, often in a
61 strain-specific manner (e.g. PfEBA-175 and GYPA; PfEBA-181 and GYPB PfEBA-140
62 and GYPC; and PfRh4 and CR1), but experimental data suggest their roles in apical
63 reorientation and host cell deformation are largely functionally redundant (Tham et al.,
64 2012).

65

66 The only receptor-ligand interaction known to be essential during the pre-invasion phase
67 involves basigin and PfRH5, which exists in a complex with PfRipr and CyRPA (Chen et
68 al., 2011; Crosnier et al., 2012; Dreyer et al., 2012; Reddy et al., 2015). Binding of the
69 PfRH5 complex to basigin is required for discharge of the rhoptry organelles into the

70 invaded cell and is associated with a calcium spike, potentially due to formation of a pore
71 at the erythrocyte surface (Volz et al., 2016; Weiss et al., 2015). Blocking the interaction
72 between PfRH5 and basigin with specific antibodies prevents invasion (Crosnier et al.,
73 2012).
74
75 Discharge of the rhoptry organelles heralds the start of active invasion. Among the
76 proteins injected from the rhoptries are those of the RON complex (RON 2, RON 4 and
77 RON5), which together form a receptor for binding by the PfAMA1 protein localized on
78 the merozoite surface (Alexander, Arastu-Kapur, Dubremetz, & Boothroyd, 2006;
79 Alexander, Mital, Ward, Bradley, & Boothroyd, 2005; Richard et al., 2010). The interaction
80 between PfAMA1 and the RON complex forms a moving junction between the parasite
81 and host cell that is believed to be entirely parasite-derived (Besteiro, Dubremetz, &
82 Lebrun, 2011; Besteiro, Michelin, Poncet, Dubremetz, & Lebrun, 2009; Harvey, Yap,
83 Gilson, Cowman, & Crabb, 2014; Koch & Baum, 2016). The moving junction provides an
84 anchoring point for the merozoite to actively invade using its own actinomyosin motor;
85 inhibiting the interaction between PfAMA1 and RON prevents invasion (Richard et al.,
86 2010; Srinivasan et al., 2011; Yap et al., 2014).
87
88 As invasion proceeds, a parasitophorous vacuole is formed from components of the host
89 cell membrane and rhoptries, yielding a protective niche for development of the new
90 daughter parasite. The third phase, echinocytosis, is a transient period of cell dehydration
91 and shrinkage observed after invasion; current evidence suggests it is triggered by
92 discharge of the rhoptry contents, prior to and independent of active invasion.

93 Echinocytosis is inhibited by reagents that prevent rhoptry discharge, such as antibodies
94 targeting basigin or PfRH5 (Weiss et al., 2015).
95
96 Most host factors known to play a role in *P. falciparum* invasion have been identified
97 based on their ability to bind to established invasion ligands or from studies of rare natural
98 mutants (Bei & Duraisingh, 2012). Given the inherent intractability of mature RBCs, which
99 lack a nucleus and DNA, the use of genetic approaches to identify and characterize
100 malaria host factors presents a logistical challenge (Egan, 2017). Recently, an shRNA-
101 based forward genetic screen using cultured red cells (cRBCs) derived ex-vivo from
102 primary human hematopoietic stem/progenitor cells (HSPCs) identified erythrocyte CD55
103 (aka DAF) as a critical host factor for *P. falciparum* invasion (Egan et al., 2015). A 70 kD
104 extracellular glycoprotein anchored to the red cell membrane by a
105 glycosylphosphatidylinositol (GPI) linkage, CD55 is broadly distributed in different tissues
106 and secretions, including blood cells (Cooling, 2015; Storry, Reid, & Yazer, 2010). On
107 erythrocytes, CD55 acts as a complement regulatory protein to prevent complement-
108 mediated damage. On epithelial cells, it has been shown to act as a receptor for Group B
109 coxsackie virus and Dr+ E. coli (Cooling, 2015; Coyne & Bergelson, 2006).
110
111 We have shown that *P. falciparum* invasion efficiency was reduced by ~50% in CD55-
112 knockdown cRBCs, and natural CD55-null erythrocytes from two rare donors with the
113 Inab phenotype were resistant to invasion (Egan et al., 2015). Importantly, the
114 requirement for CD55 was strain-transcendent, suggesting that it plays a conserved role

115 in *P. falciparum* invasion. However, the precise function of CD55 during invasion and how
116 it may interface with established ligands or receptors is unknown.
117
118 In this study, we investigated the functional role of CD55 during *P. falciparum* invasion
119 using CRISPR-Cas9 genome editing, antibody-based inhibition and live cell microscopy.
120 We found that CD55 plays a critical role during *P. falciparum* invasion of mature
121 erythrocytes, where it is specifically required for parasite internalization. As a host factor
122 that acts after discharge of the parasite's rhoptry contents, CD55 plays a unique role
123 relative to other receptors required for invasion, providing a crucial link between the
124 ligand-receptor interactions important for adhesion and deformation and effective
125 internalization.
126
127 **Results**
128 **Generation of CD55-null red blood cells using CRISPR-Cas9**
129 Previously, we observed that *P. falciparum* merozoites from several laboratory-adapted
130 strains and clinical isolates displayed impaired invasion into cryopreserved CD55-null
131 RBCs from two rare patients with the Inab phenotype (Egan et al., 2015). To study the
132 requirement for CD55 in an isogenic background, we sought to generate CD55-null
133 cRBCs from HSPCs using CRISPR-Cas9 genome editing by co-delivering single guide
134 RNAs (sgRNAs) and Cas9 in a ribonucleoprotein complex (RNP), a method that has been
135 used previously to generate null mutants in primary human CD34+ cells (Hendel et al.,
136 2015). We designed two chemically modified sgRNAs targeting the 5' end of *CD55*, and
137 delivered them individually or together into primary human $CD34^+$ HSPCs via

138 nucleofection, in complex with recombinant Cas9 (Fig. 1 A). As a control, isogenic $CD34^+$
139 HSPCs from the same donor were nucleofected with Cas9 alone. After inducing the cells
140 to differentiate down the erythroid lineage for 18 days, we observed a high percentage of
141 CD55-null cRBCs in the RNP-transfected populations; a single sgRNA targeting exon 1
142 resulted in ~70% CD55-null cRBCs, while the combination of two sgRNAs targeting exons
143 1 and 2 increased the knockout efficiency to ~90% (Figure 1B). The cells proliferated ~
144 10,000-fold and the enucleation rate was >90% in both the CD55-null cells and wild-type
145 controls, demonstrating that the progenitors differentiated efficiently and that CD55 is not
146 required for this process (Figure S1). The absence of CD55 expression in the mutant
147 cRBCs was also confirmed using immunofluorescence assays (Figure S2).
148

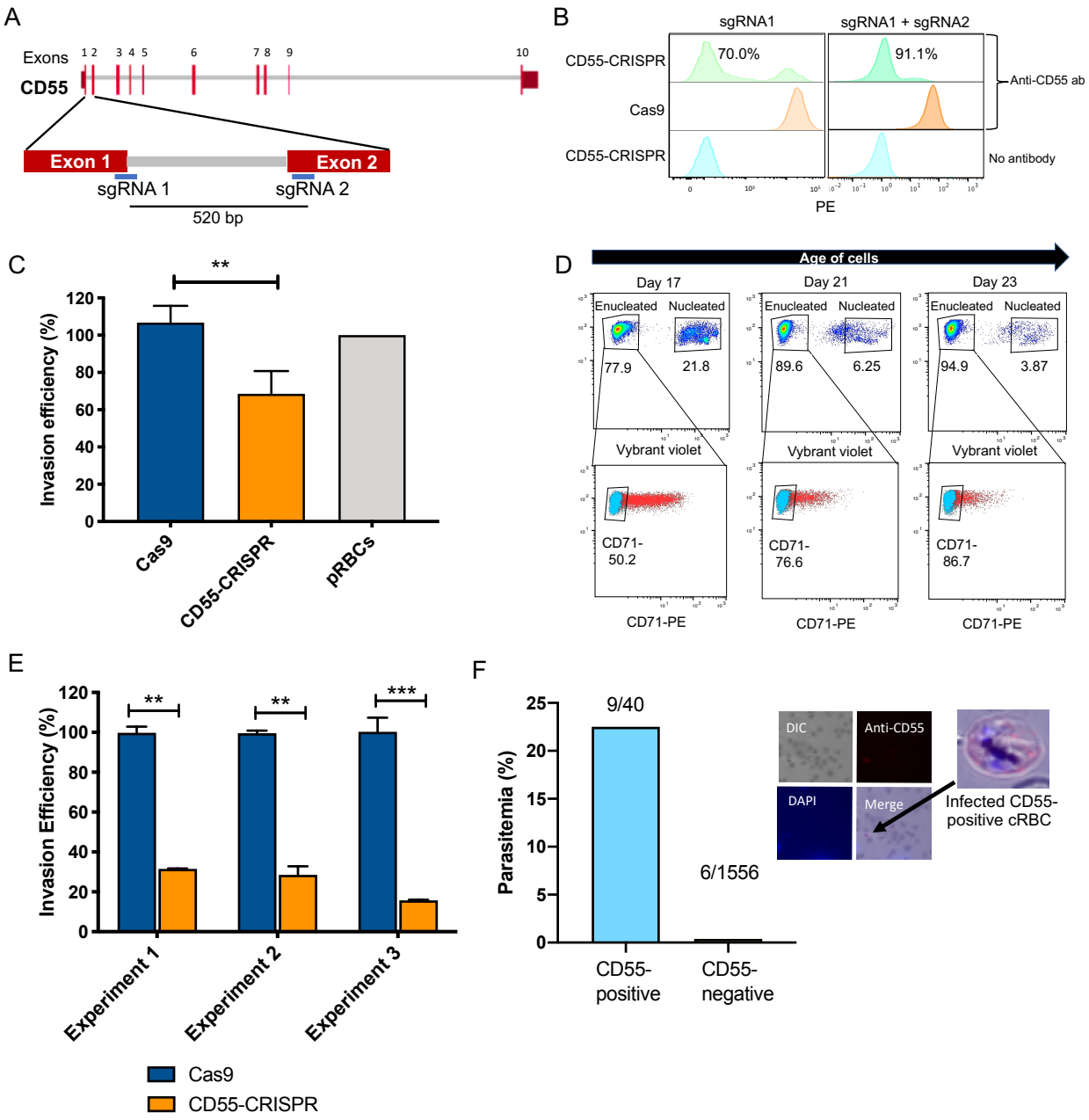

Figure 1: CD55 is required for *P. falciparum* invasion (A) Schematic of *CD55* gene structure showing targeting sites of two single guide RNAs (sgRNAs). Vertical red lines indicate the positions of *CD55* exons. (B) Expression of CD55 on mutant (CD55-CRISPR) cRBCs generated with one sgRNA (left) or two sgRNAs (right), as compared to control (Cas9) cRBCs. (C) Invasion efficiency of *P. falciparum* 3D7 in Day 18 CD55-CRISPR cRBCs compared to isogenic controls (Cas9), relative to the invasion efficiency in peripheral blood erythrocytes (N=4 biological replicates; n=3 technical replicates; error bars indicate SEM; **p<0.01). (D) Time course of expression of CD71 on cRBCs harvested on different days of differentiation. Enucleated versus nucleated cells were gated using a nuclear dye. (E) Invasion efficiency of *P. falciparum* strain 3D7 in CD71-negative, CD55-CRISPR cRBCs compared to CD71-negative isogenic controls (Cas9). Invasion

159 efficiency is presented relative to the mean of Cas9 control. Three independent biological replicates are
160 shown; error bars represent SEM (n=2 or 3 technical replicates; **p<0.01, ***p<0.005). (F) Parasitemia in
161 population of CD55-CRISPR cRBCs, in which ~90% of the cells lack CD55 (CD55-negative), and the
162 remaining are CD55-positive, as quantified by immunofluorescence assays. Below are representative
163 images of CD55-CRISPR cRBCs infected with *P. falciparum*. Images are brightfield with fluorescence
164 overlaid. Blue, dapi. Red, anti-CD55-PE.
165

166 **CD55 is required for *P. falciparum* invasion**

167 To specifically assess the requirement for CD55 for *P. falciparum* invasion, we performed
168 invasion assays using strain 3D7 in CD55-CRISPR cRBCs or in isogenic control cRBCs
169 that had been differentiated for 18 days. While invasion into the CD55-CRISPR cRBCs
170 was impaired relative to the control cells, it was only reduced by ~40% (Figure 1C). This
171 subtle phenotype was reminiscent of the results for CD55-knockdown cRBCs, and
172 differed from the strong invasion phenotype observed in erythrocytes from two CD55-null
173 patients (Egan et al., 2015). Since cRBCs are less mature than erythrocytes from
174 peripheral blood, we hypothesized that the relatively mild invasion phenotype observed
175 in the CD55-null cRBCs may be explained by the overall maturation state of the ex-vivo
176 cultures on day 18.

177

178 To begin to determine whether cell maturity modifies the requirement for CD55 during *P.*
179 *falciparum* invasion, we assessed the surface expression of CD71 in the cRBCs, which
180 is highly expressed on erythroblasts and young reticulocytes, but quickly disappears as
181 reticulocytes mature into erythrocytes (J. Hu et al., 2013). Flow cytometry on day 17
182 demonstrated that approximately 50% of the enucleated cRBCs were CD71-positive and
183 ~50% were CD71 negative, indicating a mix of cell maturity in the population (Figure 1D).
184 This was further validated using a reticulocyte stain (Figure S3), which showed that day
185 17 cells were ~ 50% reticulocytes and 50% erythrocytes. A timecourse over 7 additional
186 days of terminal differentiation revealed a progressive loss of CD71 expression,
187 consistent with a change in the population structure to one dominated by erythrocytes
188 rather than reticulocytes (Figure 1D).

189

190 To isolate a more homogeneous population of mature cRBCs for invasion assays, we
191 differentiated the cRBCs for 21-22 days and then used anti-CD71 antibody-immobilized
192 magnetic beads to enrich for CD71-negative cells (Figure S4). Using these highly mature
193 cells, invasion assays with *P. falciparum* strain 3D7 showed a ~75% reduction in invasion
194 into the CD55-CRISPR cRBCs as compared to isogenic control cRBCs in three biological
195 replicate experiments (Figure 1E). Since our CRISPR-Cas9 genome editing strategy
196 yielded a mixed population of ~90% CD55-null and 10% CD55-positive cells, we
197 suspected that the residual invasion observed in the "CD55-CRISPR" population was
198 attributable to wild-type cells. This was confirmed by immunofluorescence assays
199 showing that *P. falciparum* invasion was restricted to the cells expressing CD55: the
200 parasitemia in the minority, CD55-positive cells in the population was 22.5%, whereas
201 less than 0.5% of the CD55-null cRBCs were infected (Figure 1F). These results
202 demonstrate that CD55 is critical for *P. falciparum* invasion of fully differentiated cRBCs,
203 mimicking the prior observations with natural CD55-null erythrocytes, and validating
204 CD55 as an essential host factor for *P. falciparum* invasion. Based on previous
205 observations that the expression levels of many RBC surface proteins decline during
206 reticulocyte maturation (Chu et al., 2018; Malleret et al., 2013), we hypothesize that high
207 levels of other receptors important for invasion, such as basigin, may explain the reduced
208 requirement for CD55 for *P. falciparum* invasion of younger, CD71-positive reticulocytes.
209

210 **Antibodies targeting CD55 inhibit *P. falciparum* invasion**

211 To determine if *P. falciparum* invasion can be inhibited using antibodies targeting CD55,
212 we performed in vitro growth assays in the presence of three established anti-CD55
213 monoclonal antibodies individually and in combination. The antibodies each recognize a
214 different short consensus repeat (SCR) in the CD55 ectodomain: BRIC 230, BRIC 110
215 and BRIC 216 target SCR1, SCR2 and SCR3, respectively. While none of the antibodies
216 individually affected parasite growth, we observed a dose-dependent inhibition of parasite
217 growth over 72 hours in the presence of all three anti-CD55 monoclonal antibodies
218 combined, in comparison to an isotype control (Figure 2A). At the highest antibody
219 concentration tested (500µg/ml), the relative parasitemia was reduced by ~40% in the
220 presence of the combined monoclonals, compared to the isotype control.

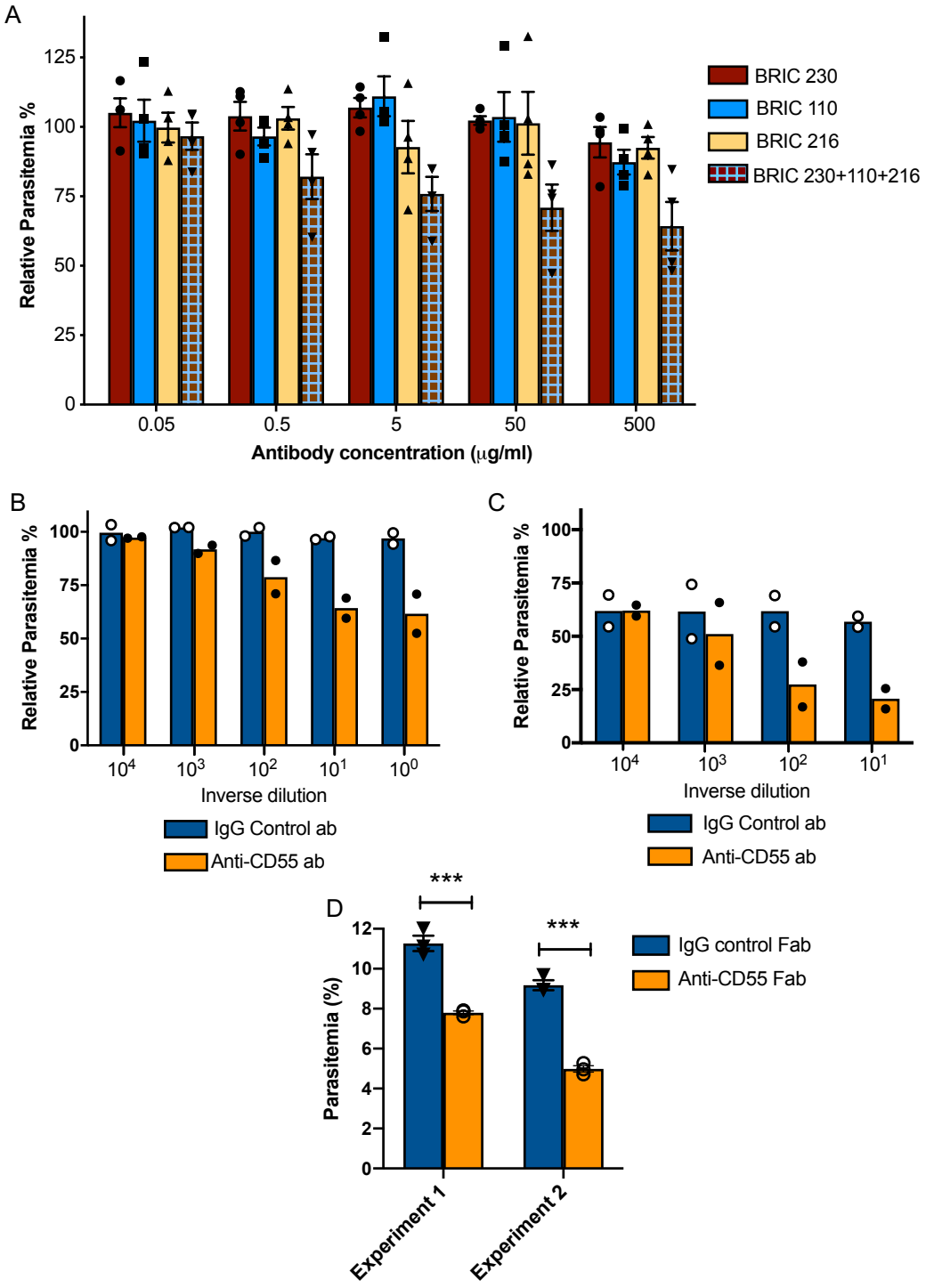

Fig 2: Blocking CD55 with antibody inhibits growth of *P. falciparum* (A) *P. falciparum* strain 3D7 parasitemia after 72 hours of growth in RBCS in the presence of increasing concentrations of anti-CD55 monoclonal antibodies, relative to isotype control antibody (BRIC 170) at the same concentration. For the pooled antibodies, the indicated concentration was the total combined value, and there were equimolar amounts of each antibody. (N=3 biological replicates; n=2 technical replicates). Error bars indicate SEM.

227 (B) Parasitemia of *P. falciparum* strain 3D7 after 72 hours growth in non-enzyme treated RBCs with
228 increasing concentrations of polyclonal anti-CD55 IgG antibody, relative to that in isotype control antibody
229 at same concentration. (N=2 biological replicates; n=2 technical replicates). The highest antibody
230 concentration (10^0) was 400 ug/ml. (C) As in B, but with neuraminidase-treated RBCs. The highest antibody
231 concentration (10^1) was 40 ug/ml. (D) *P. falciparum* strain 3D7 parasitemia after 72 hours growth in 400
232 ug/ml Fab fragments generated from anti-CD55 polyclonal antibody or isogenic control. Error bars indicate
233 SEM. ***$p<0.005$. The starting parasitemias were 0.3% (Experiment 1) or 0.5% (Experiment 2).
234

235

236 To further study anti-CD55-mediated inhibition of *P. falciparum* invasion, we generated a
237 rabbit polyclonal antibody raised against the entire ectodomain of human erythrocyte
238 CD55. Flow cytometry analysis confirmed that the purified IgG antibody recognizes an
239 antigen on wild-type (WT) RBCs but not on CD55-null RBCs from an Inab donor
240 (Takahashi, 2008), confirming its specificity for CD55 (Figure S5). In *P. falciparum* growth
241 assays, we observed a dose-dependent inhibition of parasite growth in the presence of
242 anti-CD55 antibody relative to isotype control, with a ~40% reduction in relative
243 parasitemia at the highest concentration of antibody (400 μg/ml) (Figure 2B). This degree
244 of inhibition was very similar to that seen for the pooled monoclonal antibodies; together,
245 these findings suggest that blocking CD55 on the RBC can inhibit *P. falciparum* invasion.
246
247 We next tested the effect of anti-CD55 antibody on sialic acid-independent invasion
248 pathways by treating cells with neuraminidase (NM) to remove sialic acid. As has been
249 described previously, the growth of *P. falciparum* strain 3D7 was inhibited ~40% in NM-
250 treated RBCs as compared to untreated cells in the absence of antibody (Figure 2C),
251 reflecting some reliance of strain 3D7 on sialic acid for efficient invasion. In the presence
252 of increasing concentrations of anti-CD55 antibody, we observed a dose-dependent
253 inhibition of parasite growth in the NM-treated cells that is similar to untreated cells (~60%
254 versus ~40% at maximum concentration of antibody) (Figure 2B-C). The finding that
255 CD55 blockade inhibits *P. falciparum* regardless of the presence of membrane sialic acid
256 suggests that CD55 plays a role in both sialic acid-dependent and -independent invasion.
257 These results are consistent with previous findings showing that the requirement for CD55

258 is strain-transcendent, including strains that rely on sialic acid to various degrees (Egan
259 et al., 2015).
260
261 To confirm that the inhibitory effect of the polyclonal anti-CD55 antibody on *P. falciparum*
262 growth was not due to crosslinking, we tested the growth inhibitory activity of monovalent
263 anti-CD55 antibody fragments (Fab fragments). In the presence of 400 µg/ml of anti-CD55
264 Fab fragments, we observed ~40% reduction in relative parasitemia, recapitulating the
265 growth inhibitory activity observed with the bivalent anti-CD55 IgG antibody (Figure 2D).
266 These results further support the conclusion that CD55 is a critical host receptor for *P.*
267 *falciparum*.
268
269 **Blocking CD55 inhibits *P. falciparum* internalization**
270 To specifically determine the impact of CD55 blockade on *P. falciparum* invasion, we used
271 live cell imaging to visualize and quantify schizont rupture and merozoite invasion in real
272 time in the presence of the anti-CD55 polyclonal antibody or an isotype control (Figure
273 3A; Movies S1-S2). First, we quantified the efficiency of merozoite internalization in the
274 presence of anti-CD55 antibody versus isotype control. In the presence of the isotype
275 control antibody, of 345 *P. falciparum* merozoites that contacted an RBC, 53 invaded
276 successfully (15%) (Figure 3B). This frequency is similar to that described in previous live
277 microscopy studies analyzing the efficiency of 3D7 merozoite invasion in the absence of
278 antibodies (Volz et al., 2016; Weiss et al., 2015). In comparison, merozoite invasion was
279 significantly reduced in the presence of anti-CD55 antibody. Out of 312 merozoites that
280 made contact with an RBC in the presence of anti-CD55, only 21 successfully invaded

281 (6.7%) (Figure 3B). The number of invasion events per schizont rupture was similarly
282 reduced by half in the presence of anti-CD55 compared to control antibody (Figure 3C),
283 indicating that anti-CD55 antibody inhibits entry but does not prevent initial contact
284 between the merozoite and RBC.
285
286 **Blocking CD55 has no impact on pre-invasion kinetics**
287 Next, we examined the impact of CD55 blockade on the kinetics of the three main phases
288 of *P. falciparum* invasion: the pre-invasion time (period from initial contact to the onset of
289 internalization), the internalization time, and the time to echinocytosis (transient period of
290 cell dehydration that occurs after internalization) (Dvorak, Miller, Whitehouse, & Shiroishi,
291 1975; Weiss et al., 2015). For the subset of merozoites that ultimately invaded
292 successfully, there was no difference in the length of the pre-invasion time, internalization
293 time, or time to echinocytosis in the presence of anti-CD55 antibody compared isotype
294 control (Figure 3D-F). These results indicate that blocking CD55 does not impact pre-
295 invasion kinetics, at least not for the merozoites that manage to invade in the presence
296 of antibody.
297

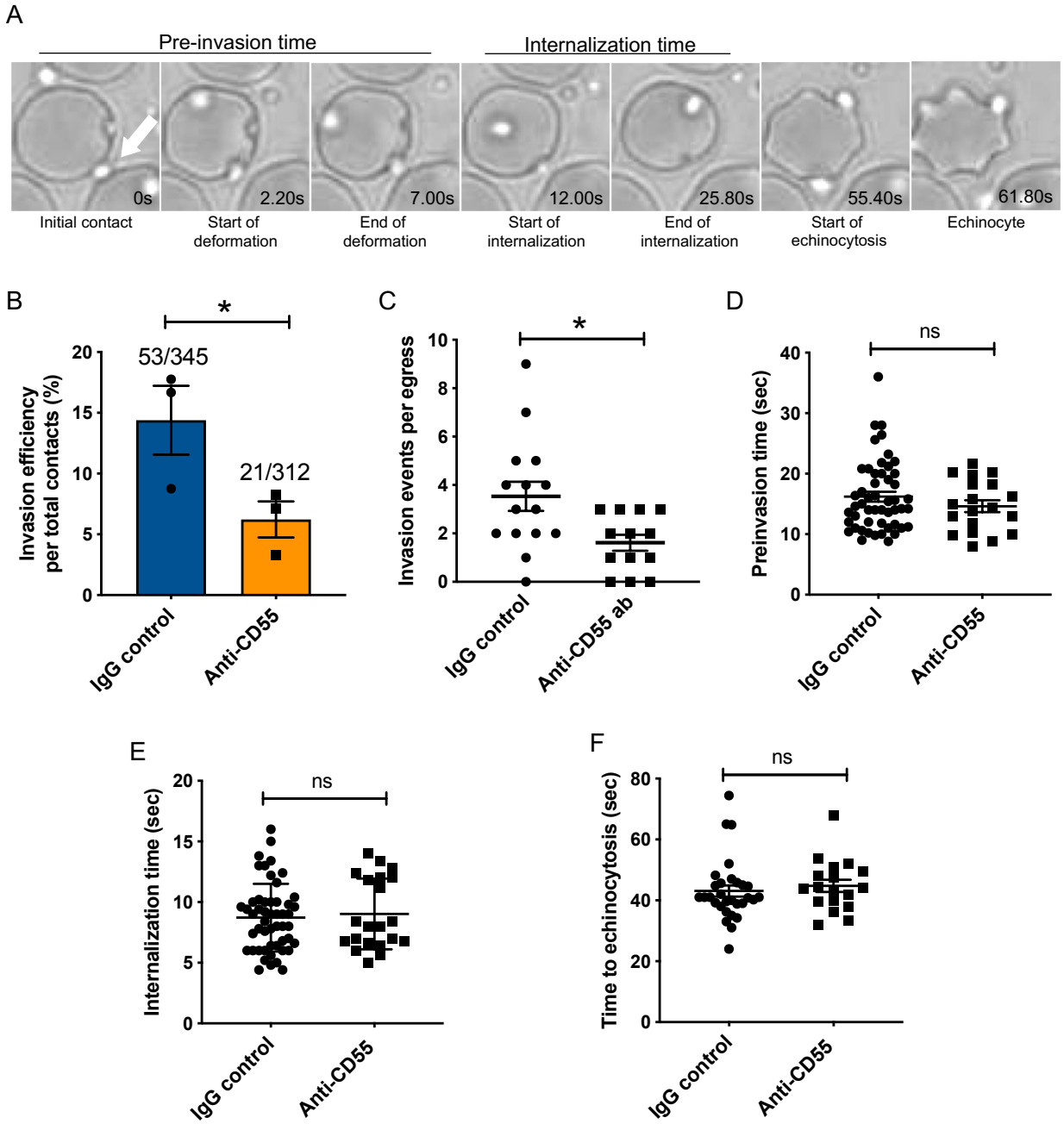

Fig 3: Blocking CD55 with antibody inhibits invasion but not pre-invasion kinetics (A) Time-lapse images of invasion after initial merozoite contact. Arrowhead indicates invading merozoite. Time in seconds. (B) Percentage of merozoites that invaded an RBC after initial contact in presence of polyclonal anti-CD55 antibody (anti-CD55) or isotype control (IgG control). Bottom number is the total number of merozoites followed that made contact with the RBC, and top number is the subset that invaded. The data were acquired in three independent experiments, and the dots indicate the mean invasion efficiency from each experiment; *p=0.03. (C) Number of successful invasion events per schizont rupture (egress) in presence of anti-CD55 antibody or isotype control; *p=0.01. (D) Pre-invasion time (in seconds) for merozoites that

307 contact an RBC in the presence of anti-CD55 antibody or isotype control. (E) Internalization time (in
308 seconds) for merozoites in the presence of anti-CD55 antibody or isotype control antibody. (F) Time to
309 echinocytosis from the end of merozoite internalization in the presence of anti-CD55 antibody or isotype
310 control. Error bars indicate SEM; ns, not significant (B-F).
311

312 **Merozoite-induced erythrocyte deformation is unaffected by CD55 blockade**

313 During the pre-invasion period, parasite attachment to the RBC is associated with
314 substantial deformation of the host cell membrane as the merozoite reorients apically
315 (Dvorak et al., 1975; Gilson & Crabb, 2009; Paul et al., 2015). The degree of deformation
316 is variable, and is mediated by interactions between parasite ligands released from the
317 apical microneme organelles, such as the EBAs and Rhs, and receptors on the RBC
318 membrane (Weiss et al., 2015). To investigate whether CD55 plays a role in RBC
319 deformation, we used live microscopy to quantitate the efficiency and kinetics of
320 merozoite-induced RBC deformation in the presence of anti-CD55 antibody versus
321 isotype control. The efficiency of deformation was similar in the presence of the two
322 antibodies: approximately 67% of merozoites deformed the RBC in the presence of anti-
323 CD55 antibody, compared to ~60% deformation efficiency with the isotype control (Figure
324 4A). In addition, there was no significant difference in the duration of the deformation
325 period in the presence of the two different antibodies (Figure 4B), suggesting that CD55
326 does not influence merozoite-induced deformation.

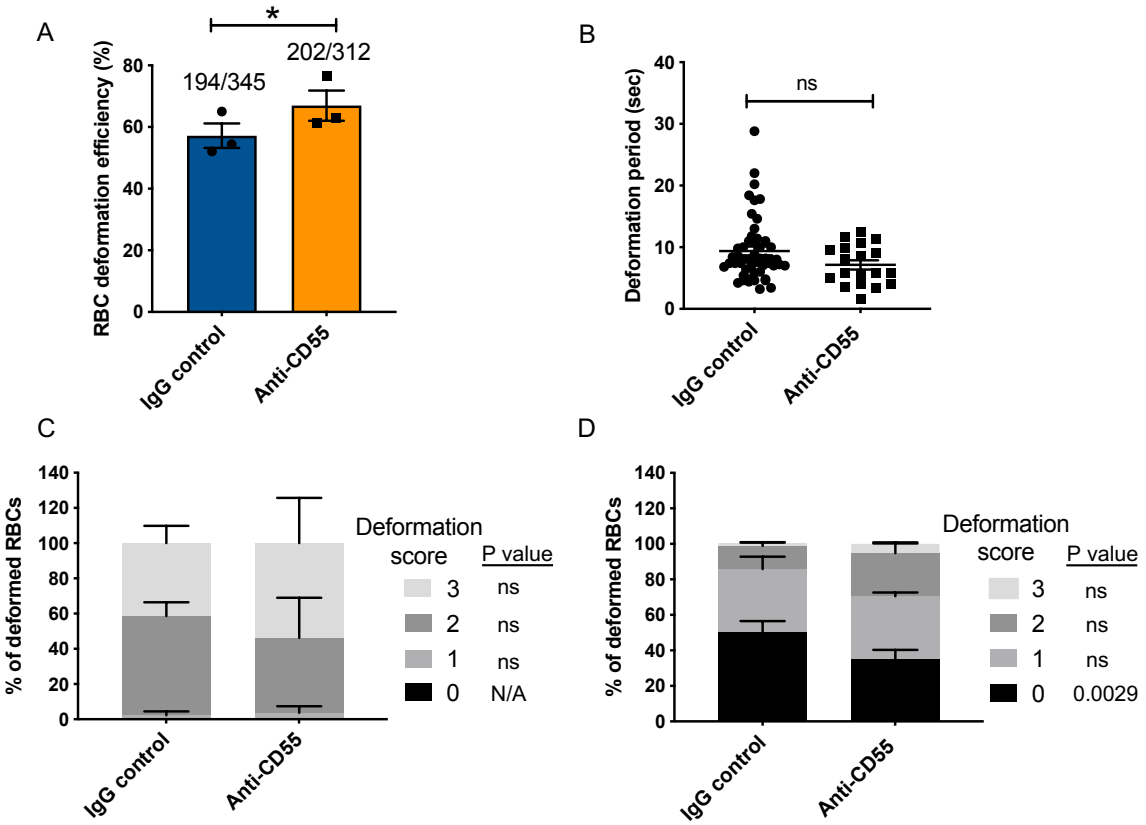

Fig 4: Merozoite-induced erythrocyte deformation is not affected by blocking CD55 (A) Efficiency of RBC deformation by merozoites that make contact in presence of anti-CD55 or IgG control. The fractions indicate the number of deformed RBCs out of the total merozoite-RBC contacts observed. The data were acquired in three independent experiments, and the dots represent the mean for each experiment.; *p=0.02. **(**B) Duration of erythrocyte deformation induced by attached merozoites that ultimately invaded in presence of polyclonal anti-CD55 antibody (anti-CD55) or isotype control (IgG control). Time in seconds. (C-D) Strength of merozoite-induced deformation in presence of anti-CD55 or isotype control for cases where invasion was successful (C) or not successful (D); N/A, not applicable; ns, not significant, *p=0.0029. Error bars indicate SEM (A-D).

338 We employed a four-point deformation scale to quantify the intensity of merozoite-induced
339 RBC deformation in the presence of antibody, where 0 denotes the absence of
340 deformation and 3 denotes the most extreme degree of deformation (Weiss et al., 2015)
341 (Movies S3-S5). Almost all merozoites that invaded successfully induced strong
342 deformation (scores of 2 or 3), regardless of which antibody was present (Figure 4C). In
343 comparison, merozoites that failed to invade had lower deformation scores, the majority
344 having scores of 0 or 1. For these merozoites, the distribution of scores skewed higher
345 in the presence of anti-CD55 antibody compared to the isotype control, perhaps reflecting
346 the inability of otherwise "fit" merozoites to complete invasion (Figure 4D). Taken
347 together, these findings demonstrate that blocking CD55 with antibody does not influence
348 the efficiency, duration, or strength of merozoite-induced RBC deformation, and instead
349 suggest that CD55 exerts its effect on invasion at a downstream step.
350
351 To further validate the conclusions of the antibody inhibition experiments, we took a
352 complementary approach and performed live cell imaging of *P. falciparum* invasion with
353 natural CD55-null erythrocytes from a rare donor with the Inab phenotype, where CD55
354 is absent due to a stop codon in exon 2(Takahashi, 2008). In traditional invasion assays,
355 we observed ~80% reduction in the efficiency of *P. falciparum* invasion into CD55-null
356 RBCs as compared to control RBCs after ~ 18 hours, as has been shown previously
357 (Egan et al., 2015) (Figure S6). When imaging invasion in real time, we did not observe
358 any successful invasion events into the CD55-null RBCs, out of 310 merozoites that made
359 contact (Figure 5A and Movies S6-S7). In comparison, there were 25 successful invasion
360 events into the control RBCs, out of 197 merozoites that made contact (~11%). Although

361 invasion into the CD55-null cells was clearly impaired, there was no difference in the
362 efficiency of merozoite-induced RBC deformation between the two genetic backgrounds
363 (Figure 5B). Moreover, we observed no significant difference in the distribution of
364 deformation scores between CD55 null and control RBCs for merozoites that did not
365 invade (Figure 5C). These results are consistent with the findings from the antibody
366 inhibition experiments, and suggest that CD55 influences invasion by acting after the
367 period of erythrocyte deformation.

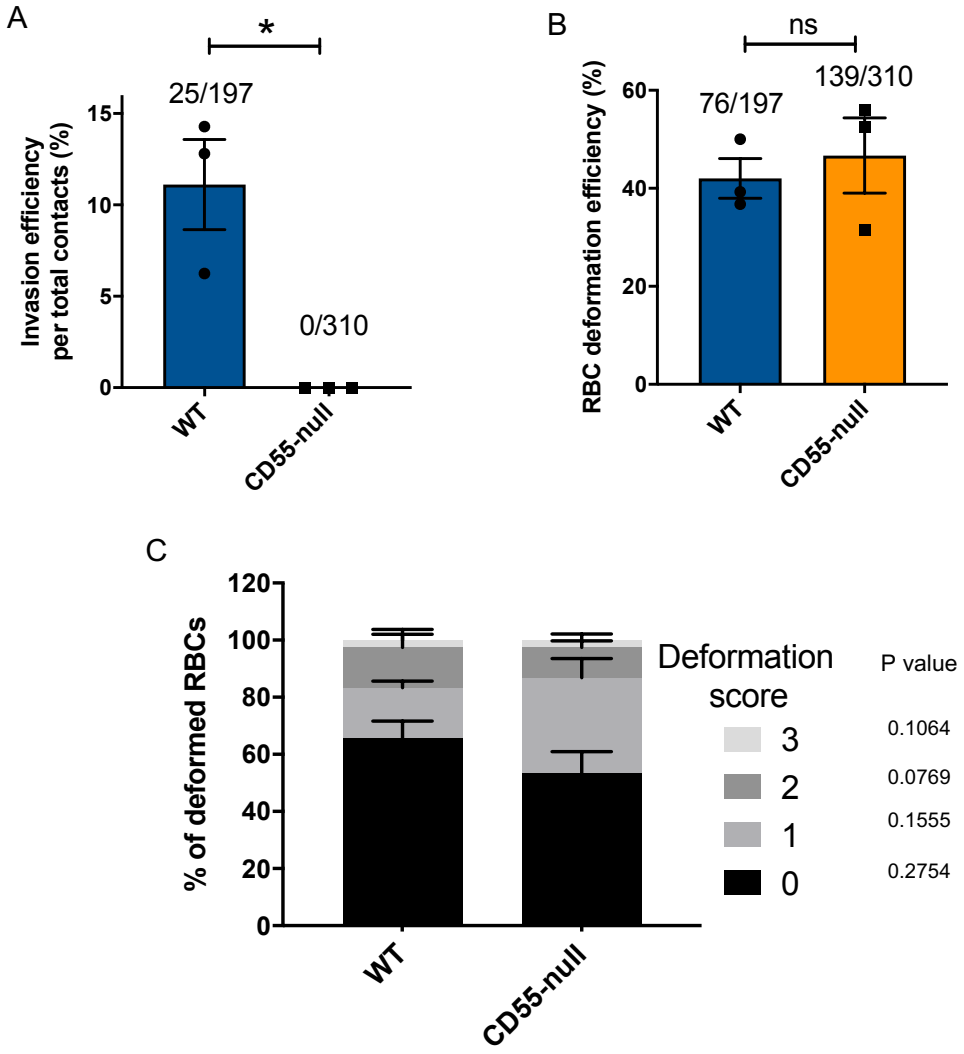

368

369 **Fig 5: Absence of CD55 prevents invasion but does not impact deformation. (**A) Percentage of
370 merozoites that invaded wild-type (WT) or CD55-null RBCs after initial contact. Bottom number is the total

371 number of merozoites followed that made contact with the RBC, and top number is the subset that invaded.
372 The data were acquired in three independent experiments, and the dots indicate the mean invasion
373 efficiency from each experiment; *p=0.04. (B) Efficiency of WT or CD55-null RBC deformation upon
374 merozoite contact. Bottom number is the total number of RBCs contacted by a merozoite, and top number
375 is the subset that were deformed upon contact. The data were acquired in three independent experiments,
376 and the dots indicate the mean deformation efficiency for each experiment; ns, not significant. (C) Strength
377 of merozoite-induced deformation of WT or CD55-null RBCs among non-invading merozoites; ns, not
378 significant. Error bars indicate SEM (A-C).
379

380

381 **CD55 acts downstream of rhoptry discharge**

382 Since we observed that the blocking or deletion of CD55 impaired *P. falciparum* entry
383 without altering pre-invasion kinetics or membrane deformation, we hypothesized that
384 CD55 functions after the ligand-receptor interactions that mediate attachment and
385 deformation. During the sequential steps of *P. falciparum* invasion, RBC deformation is
386 followed by injection of the rhoptry organelle contents into the host cell cytoplasm, an
387 event that requires an interaction between the parasite ligand PfRh5 and its RBC
388 receptor, basigin (Weiss et al., 2015). The contents of the rhoptries in turn are believed
389 to trigger echinocytosis. When the interaction between PfRH5 and basigin is blocked
390 using inhibitory antibodies and rhoptry discharge is prevented, echinocytosis fails to occur
391 (Volz et al., 2016; Weiss et al., 2015). To investigate whether CD55 is similarly required
392 for release of the rhoptry contents, we quantified the incidence of RBC echinocytosis
393 elicited by attached merozoites in the presence of anti-CD55 antibody versus isotype
394 control using a cytochalasin-D (cyt-D) live microscopy assay (Figure 6A-B and Movie S8).
395 Cyt-D is an inhibitor of actin polymerization that prevents merozoite internalization by
396 inhibiting the actino-myosin motor, but does not impact attachment, rhoptry discharge, or
397 echinocytosis (Miller, Aikawa, Johnson, & Shiroishi, 1979; Weiss et al., 2015). Upon
398 treatment with cyt-D, ~60% of merozoites that attached to an RBC triggered echinocytosis
399 in the presence of the isotype control antibody, and a similar rate of echinocytosis was
400 observed in the presence of anti-CD55 antibody (Figure 6C). These results demonstrate
401 that blocking CD55 does not significantly impact rhoptry discharge or echinocytosis,
402 standing in distinct contrast to what has been observed for basigin and Rh5, where
403 blocking their interaction with antibodies prevents echinocytosis (Weiss et al., 2015).

404 Together, these findings demonstrate that CD55 acts downstream of the interaction
405 between RH5 and basigin, facilitating a step of invasion that occurs after release of the
406 rhoptry organelles.

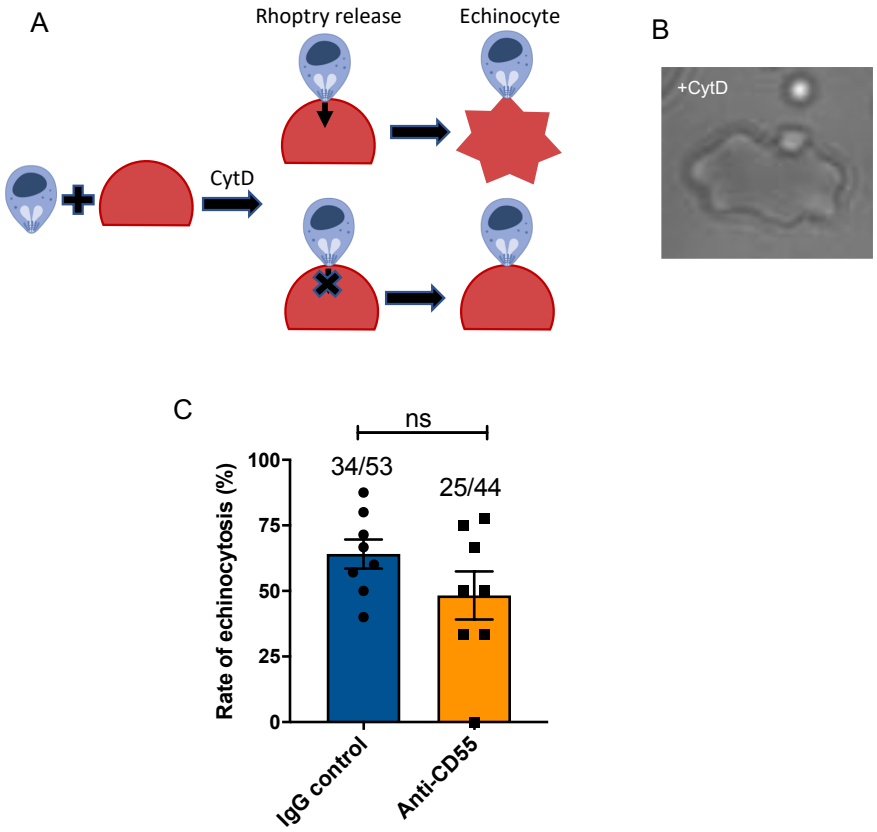

Fig 6: Blocking CD55 with antibody does not impact echinocytosis. (A) Cartoon illustrating echinocytosis elicited by an attached merozoite that has discharged its rhoptry contents in the presence of cyt-D, which prevents internalization. Reagents that block rhoptry discharge prevent echinocytosis. (B) Image showing an echinocyte with an attached merozoite. Scale bar=5um. (C) Echinocytosis efficiency in the presence of anti-CD55 antibody or isotype control. Bottom number is the total number of merozoite-RBC pairs observed to make contact, and top number is the subset in which echinocytosis occurred. The data are from eight independent experiments. Dots indicate the mean from each experiment and error bars represent the standard error of mean; ns, not significant.

407

408

409 **CD55 may be required for progression of the moving junction**

410 The moving junction that forms between the cell membranes of an invading merozoite
411 and the erythrocyte during internalization involves interactions between PfAMA1, which
412 derives from the micronemes, and the PfRON complex, which is expressed by the
413 rhoptries. To investigate a possible role for CD55 in formation of the moving junction, we
414 sought to visualize PfAMA1 and PfRON4 as merozoites attempted to invade CD55-null
415 (Inab) or wild-type erythrocytes in the presence of cyt-D. Under these conditions, we
416 observed a ~50% reduction in the efficiency of merozoite attachment to CD55-null
417 erythrocytes as compared to WT controls by flow cytometry, as has been observed
418 previously (Figure 7A) (Egan et al., 2015). Using confocal microscopy, we found that
419 PfAMA1 and PfRON4 were frequently co-localized at the cellular interface for merozoites
420 attached to WT control cells (~85%) (Figure 7B). In comparison, for merozoites attached
421 to CD55-null erythrocytes, PfAMA1 and PfRON4 were co-localized at the cellular
422 interface in only ~40% of cases (Figure 7B). For those merozoites in which PfAMA1 and
423 PfRON4 were colocalized at the interface, we observed that approximately half of the WT
424 control cells had an indentation at the point of merozoite contact, suggesting the
425 merozoites were mid-invasion, whereas this was never observed for the CD55-null cells
426 (Figure 7C). Together, these results support a model where CD55 is required for
427 progression of the moving junction, and acts downstream of and distinctly from all other
428 known host receptors for *P. falciparum* invasion.

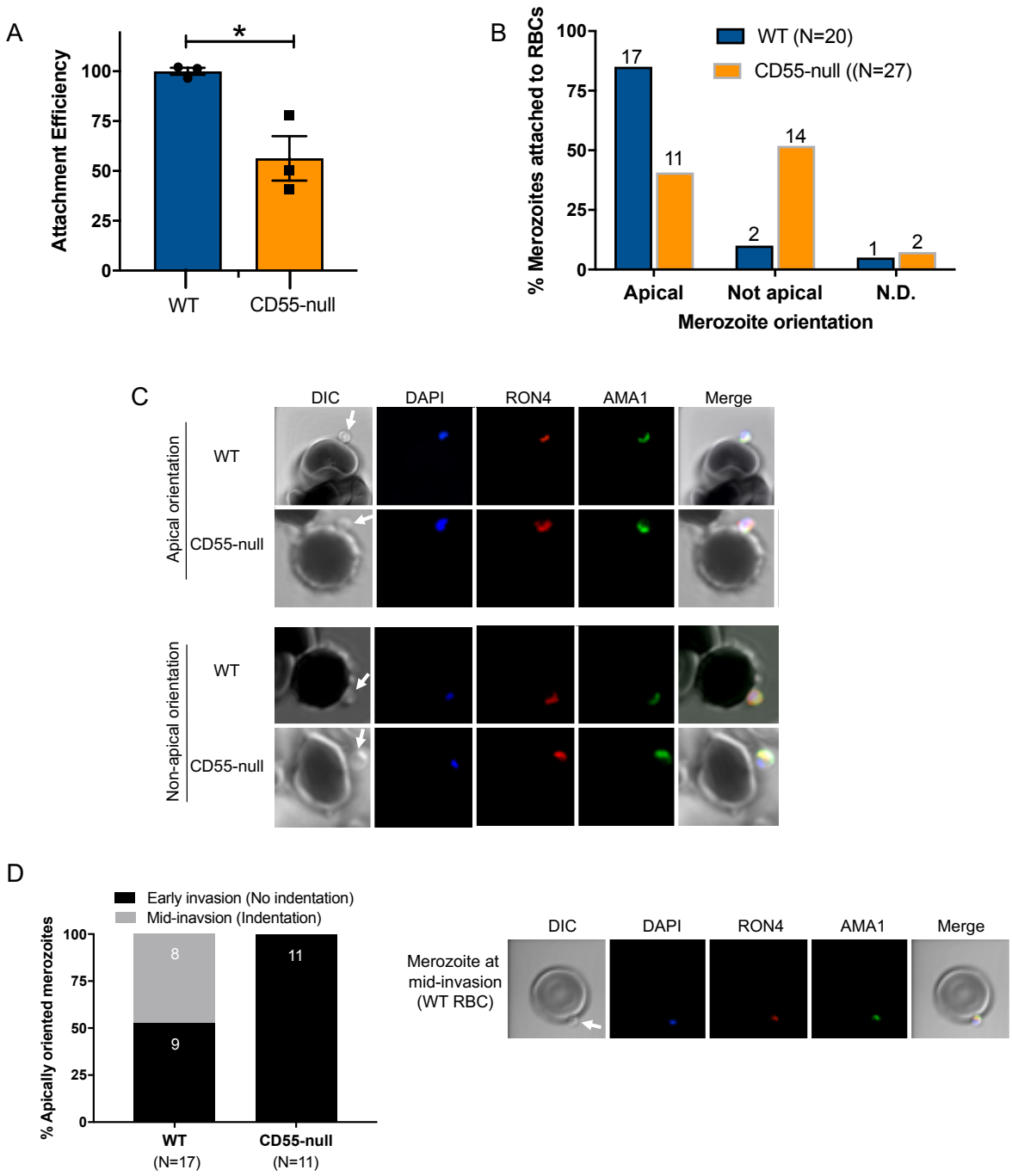

Fig 7: Invasion fails to progress in the absence of CD55.

(A) Attachment efficiency of *P. falciparum* merozoites to CD55-null versus control RBCs in the presence of cyt-D, as measured by flow cytometry 90 min after the addition of synchronized schizonts (N=3, n=3). Error bars indicate SEM; *p<0.018. (B) Orientation of merozoites attached to WT versus CD55-null RBCs, indicated by the localization of AMA1, RON4, and a density at the merozoite's apical end as measured by confocal microscopy. Apical, AMA1 and RON4 co-localized at the cellular interface and merozoite density abutting RBC; Not apical, AMA1 and RON4 not co-localized at the cellular interface and merozoite density

437 not abutting RBC; N.D., indeterminate. The numbers above each bar indicate the subset of attached
438 merozoites in that orientation. (C) Representative confocal images showing merozoites attached to RBCs
439 with apical or non-apical orientation. Merozoite density at the apical end of the merozoite is indicated by an
440 arrow. (D) Progression of invasion for merozoites apically attached to CD55-null or WT RBCs in the
441 presence of cyt-D. Panel on the right shows representative confocal images of a merozoite at the mid-
442 invasion stage.
443

444 **Discussion**

445 A comprehensive understanding of the molecular interactions required for *P. falciparum*
446 invasion has been limited by the absence of a robust genetic system to study red cells,
447 which are terminally differentiated and lack a nucleus and DNA. Previously, an RNAi-
448 based forward genetic screen in cultured red cells derived from HSPCs identified two new
449 candidate host factors for invasion: CD44 and CD55 (Egan et al., 2015). In this study, we
450 used a combination of genetics and inhibitory antibodies to determine the precise steps
451 of *P. falciparum* invasion during which CD55 functions. We have demonstrated that CD55
452 is specifically required for merozoite internalization, and plays a unique role relative to the
453 other host receptors known to act during invasion.

454 Prior work has shown that the efficiency of *P. falciparum* infection is reduced by ~
455 50% in CD55-deficient cRBCs where expression is downregulated using shRNAs. While
456 experiments using erythrocytes from two rare, CD55-null donors suggested that CD55 is
457 essential for *P. falciparum* invasion, this has never been demonstrated genetically. A
458 major roadblock to such experiments has been the technical challenges associated with
459 CRISPR-Cas9 genome editing in primary human hematopoietic stem cells, including
460 cytotoxicity from nucleic acids and low rates of transfection (Hendel et al., 2015). In this
461 study, we showed for the first time that fully mature, CD55-null cRBCs can be generated
462 efficiently from primary human HSPCs using CRISPR-Cas9 genome editing. Using
463 isogenic wild-type and mutant cells, we have demonstrated that CD55-null cRBCs are
464 resistant to *P. falciparum* invasion, confirming that CD55 is an essential host factor for *P.*
465 *falciparum*.

466

467 Here, we demonstrated the feasibility and benefits of generating truly mature erythrocytes
468 ex-vivo for the study of malaria host factors, as these cells closely mimic the target cell
469 for *P. falciparum* in the human bloodstream. Our approach involving the co-delivery of
470 two chemically modified sgRNAs together with Cas9 as a ribonucleoprotein complex has
471 been shown to be an effective strategy for CRISPR-based gene knockout in primary
472 HSPCs and T cells (Hendel et al., 2015). This method obviates the toxicity associated
473 with plasmid delivery, minimizes off-target activity, and improves sgRNA stability.
474 Combined with our ex-vivo erythropoiesis culture system, this method can efficiently
475 generate terminally differentiated, enucleated, CD71-low red cells with a high rate of gene
476 knock out that can be used to study host genetic determinants for *P. falciparum* in an
477 isogenic background.
478
479 We observed that the reliance of *P. falciparum* on CD55 for invasion increased
480 significantly as enucleated cRBCs matured into erythrocytes, likely reflecting the
481 substantial changes in protein abundance that occur during terminal maturation of human
482 red cells, including for proteins known to act as receptors, such as basigin and CR1
483 (Gautier et al., 2016; G. Hu et al.). The efficiency of *P. falciparum* invasion is further
484 influenced by the deformability of the red cell membrane (Tiffert et al., 2005), a biophysical
485 property that also changes as red cell progenitors proceed through enucleation and final
486 maturation (Giarratana et al., 2005). As clinical malaria is primarily a disease of mature,
487 peripheral blood erythrocytes, our results showing that terminal red cell maturation
488 modifies the requirement for CD55 during invasion highlights the potential drawbacks of
489 using cell lines to study host factors for *P. falciparum*. While considered erythroid in

490 nature, immortalized cell lines such as JK-1, EJ and BEL-A have low rates of enucleation
491 and terminal maturation (Kanjee et al., 2017; Satchwell et al., 2019; Scully et al., 2019),
492 suggesting their utility for genetic experiments on *P. falciparum* invasion may be limited
493 by incomplete phenotypes.
494
495 Antibodies targeting a variety of specific host receptors for *P. falciparum* have been
496 shown to have invasion inhibitory activity, including those against GYPA, CR1, and
497 basigin (Crosnier et al., 2012; Pasvol et al., 1989; Spadafora et al., 2010). While we found
498 that individual monoclonal antibodies against three distinct SCR domains of CD55 had
499 no discernable effect on *P. falciparum* growth, in combination they had potent dose-
500 dependent inhibitory activity, suggesting CD55's role in invasion is not restricted to a
501 specific SCR domain. Our demonstration that both the polyclonal anti-CD55 antibody and
502 anti-CD55 Fab fragments can inhibit *P. falciparum* growth aligns with the results from our
503 genetic studies, and corroborates the conclusion that CD55 is a critical host factor for *P.*
504 *falciparum*. In contrast to CR1, where antibodies are only inhibitory in the absence of red
505 cell sialic acid (Spadafora et al., 2010), anti-CD55 antibody blocked both sialic acid-
506 dependent and -independent invasion. This finding is consistent with prior studies
507 showing that the requirement for CD55 in *P. falciparum* invasion is strain-transcendent
508 (Egan et al., 2015), and implies a model where CD55 acts distinctly from CR1 and the
509 other alternative, strain-specific receptors.
510
511 Given the inherent limitations associated with studying invasion on a population scale in
512 longer term assays, live microscopy has been increasingly employed to visualize

513 individual *P. falciparum* invasion events in real time. Analysis of the morphology and
514 kinetics of discrete invasion steps in the context of blocking antibodies or soluble proteins
515 has contributed to a model describing the molecular events that occur during invasion
516 (Volz et al., 2016; Weiss et al., 2015). Our live microscopy experiments have added a
517 new dimension to this model by revealing that merozoite internalization is inhibited in the
518 presence of anti-CD55 antibody or with CD55-null erythrocytes, demonstrating for the first
519 time that CD55 is specifically required for parasite entry. Where and how does CD55 act
520 in relation to the *P. falciparum* ligands and erythrocyte receptors known to function during
521 invasion? We observed no impact of the anti-CD55 antibody on pre-invasion kinetics or
522 merozoite-induced erythrocyte deformability, findings that were validated using CD55-null
523 erythrocytes from a rare donor. These results suggest that CD55 functions distinctly from
524 the "alternative" receptors required for apical reorientation and red cell deformation (e.g.
525 glycophorins and CR1), as blocking interactions between these receptors and their
526 ligands strongly inhibits merozoite-induced deformability (Weiss et al., 2015).
527
528 Echinocytosis is a phenomenon of transient red cell shrinkage that commences soon after
529 merozoite internalization. Current evidence suggests that it is stimulated by changes in
530 the red cell cytoplasm that occur once an irreversibly-attached merozoite discharges its
531 rhoptry contents into the erythrocyte (Volz et al., 2016; Weiss et al., 2015). Echinocytosis
532 is inhibited by antibodies that block the interaction between PfRH5 and basigin, implying
533 that this interaction is necessary for rhoptry discharge (Weiss et al., 2015). These blocking
534 antibodies also inhibit Ca^{2+} flux into the erythrocyte, possibly reflecting formation of a pore
535 at the cellular interface when PfRH5 and basigin interact (Volz et al., 2016). The

536 glycophorins and CR1 act early in the pre-invasion phase during apical reorientation, and
537 blocking their interactions with ligands using genetics, enzyme treatments, or antibody
538 blockade also inhibits echinocytosis (Volz et al., 2016; Weiss et al., 2015). In contrast,
539 echinocytosis is not prevented by treatment with the actin polymerization inhibitor cyt-D
540 or reagents that block the interaction of PfAMA1 and the RON complex. Together, these
541 findings demonstrate that the stimulus for echinocytosis occurs after the interaction of
542 PfRH5 with basigin, but before establishment of the moving junction.
543
544 Our observation that anti-CD55 antibody had no effect the efficiency of merozoite-induced
545 echinocytosis demonstrates that CD55 acts distinctly from basigin and the other
546 established host receptors known to act during *P. falciparum* invasion. While both anti-
547 CD55 and anti-basigin inhibit invasion, echinocytosis occurs normally in the presence of
548 anti-CD55 but is blocked by anti-basigin antibody, likely due to inhibition of rhoptry
549 discharge (Volz et al., 2016). As blocking CD55 does not inhibit deformation nor
550 echinocytosis during invasion, our findings support a model in which CD55 acts after
551 rhoptry discharge, and specifically impacts merozoite internalization.
552
553 Merozoite internalization requires the formation of a moving junction between the cell
554 membranes of the invading merozoite and the erythrocyte that moves posteriorly down
555 the parasite as it invades. The current model of the moving junction involves interactions
556 between PfAMA1 expressed on the merozoite surface and the PfRON complex inserted
557 into the red cell membrane, independent of any host-encoded receptors (Alexander et al.,
558 2006; Alexander et al., 2005; Besteiro et al., 2009; Richard et al., 2010; Riglar et al., 2011;

559 Srinivasan et al., 2011). In addition to its key role in internalization, the moving junction
560 has also been proposed to be important for formation of the parasitophorous vacuole (PV)
561 (Yap et al., 2014).
562
563 Could CD55 function as a component of the moving junction during invasion? We
564 observed that PfAMA1 and PfRON4 were almost always co-localized at the cellular
565 interface for merozoites attempting to invade WT cells, whereas this was significantly less
566 common for merozoites attempting to invade CD55-null erythrocytes. For the minority of
567 merozoites that attached to CD55-null erythrocytes and had PfAMA1 co-localized with
568 RON at the cellular interface, none were observed to have progressed past early invasion,
569 unlike those attached to WT cells. Together, these findings support a model in which
570 CD55 is required for progression of the moving junction, either directly or indirectly. Future
571 studies involving higher resolution microscopy such as cryo-EM will be necessary to
572 better characterize how absence of CD55 may impact the moving junction or architecture
573 of the PV after invasion.
574
575 Our findings showing that the function of CD55 during invasion can be narrowed to the
576 internalization step are consistent with a model where CD55 acts distinctly from the other
577 known receptors for invasion, potentially by interacting with a specific parasite ligand. As
578 there is a precedent for CD55 on epithelial cells to act as a pathogen receptor that
579 transmits signals to the host cell (Coyne & Bergelson, 2006), it is tantalizing to
580 hypothesize that this molecule functions similarly in *P. falciparum* invasion of
581 erythrocytes. Ultimately, biochemical identification of parasite and erythrocyte interaction

582 partners of CD55 will yield important additional insights into the molecular function of
583 CD55 during merozoite internalization. Given the complexity of *P. falciparum* invasion and
584 the unique and essential role of CD55 relative to other established receptors, targeting its
585 activity or interaction partners in novel intervention strategies may enhance the
586 effectiveness of future therapies or vaccines for malaria.
587
588 **Methods**
589 ***P. falciparum* culture, invasion assays and growth inhibition assays**
590 *P. falciparum* strain 3D7, a laboratory-adapted strain obtained from the Walter and Eliza
591 Hall Institute (Melbourne, Australia) was routinely grown in human erythrocytes (Stanford
592 Blood Center) at 2% hematocrit in complete RPMI-1640 supplemented with 25 mM
593 HEPES, 50 mg/L hypoxanthine, 2.42 mM sodium bicarbonate and 0.5% Albumax
594 (Invitrogen) at 37°C in 5% CO_2 and 1% O_2.
595
596 Parasite invasion assays were performed using synchronized late-stage schizont
597 parasites isolated using a MACS magnet (Miltenyi) and added at 1.0-1.5% initial
598 parasitemia to the cultured red blood cells (cRBCs) or peripheral red blood cells (pRBCs)
599 at 0.3% hematocrit. For some invasion assays, cRBCs were enriched for the CD71
600 negative population by using anti-CD71 antibody immobilized magnetic beads (Miltenyi),
601 as described below. Assays were performed in a volume of 100 μl per well in a 96 well
602 plate, or at 50 μl per well in Half Area 96-well plates (Corning) for the assays with CD71-
603 negative cRBCs. The ring stage parasitemia was determined after 18-24 hours by bright-
604 field microscopy of cytospin preparations stained with May-Grünwald and Giemsa. A

605 minimum of 1000 cells were counted for each technical replicate. For assays in which
606 there was no selection for CD71-negative cells, the invasion efficiency was determined
607 by normalizing the average ring stage parasitema in each genetic background to the
608 average ring stage parasitemia in control peripheral blood RBCs (pRBCs) for each
609 biological replicate. For assays that used CD71-negative cRBCs, the ring stage
610 parasitema for each genetic background was normalized to the mean for the control
611 cRBCs. Assays were performed at least 3 times using 2-3 technical replicates.
612
613 Antibody inhibition assays were performed using pRBCs in the presence of mouse
614 monoclonal antibodies obtained from IBGRL (BRIC 216, BRIC 230, BRIC 110, BRIC
615 170), polyclonal anti-CD55 antibody produced by New England Peptide, or isotype control
616 rabbit IgG antibody (Novus). All antibodies were dialyzed overnight in RPMI buffer prior
617 to use. Schizont stage parasites were added to untreated or neuraminidase treated
618 pRBCs at 0.5% hematocrit at an initial parasitemia of 0.5% in the presence of 0.05 to 500
619 µg/ml of the antibodies. For the neuraminidase treatment, the cells were incubated with
620 66.7mU/ml of neuraminidase from *Vibrio cholerae* (Sigma) at 37°C for 1 h with shaking
621 and washed 3 times in buffer before use in the growth inhibition assays. Some assays
622 were performed in presence of Fab fragments of anti-CD55 or isotype control IgG
623 antibodies at the concentration of 400 µg/ml. The Fab fragments were prepared as
624 described below. Assays were performed 2-3 times with 2-3 technical replicates in a
625 volume of 100 µl per well in 96 well plates. Parasitemias were determined on day 3 by
626 staining with SYBR Green 1 nucleic acid stain (Invitrogen) at 1:2000 dilution in PBS/0.3%

627 BSA for 20 minutes, followed by flow cytometry analysis on a MACSQuant flow cytometer
628 (Miltenyi).
629
630 **Generation of Fab fragments**
631 Polyclonal anti-CD55 antibody and control IgG were digested using the Pierce™ Fab
632 preparation kit (Thermo Fisher Scientific). The resulting Fab fragments were quantified
633 on a spectrophotometer, concentrated, and buffer exchanged with incomplete RPMI
634 using 30K Amicon Ultra 0.5 ml centrifugal filter (Millipore). For final quantification, the Fab
635 fragments were stained with Coomassie in a 10% SDS-PAGE gel along with known
636 concentrations of the undigested antibodies, and concentrations of the Fab fragments
637 were determined using ImageJ 1.50i(Schneider, Rasband, & Eliceiri, 2012).
638
639 **Generation of cultured red blood cells from primary human CD34+ HSPCs**
640 Bone marrow-derived primary human CD34+ HSPCs (Stem Cell Technologies) were
641 cultured in erythroid differentiation medium (cPIMDM) composed of Iscove Basal Medium
642 (IMDM) (Biochrom) supplemented with 4mM L-Glutamine (Sigma), 330 µg/ml holo-
643 transferrin (BBI Solutions), 10 µg/ml of recombinant human insulin (Sigma), 2 IU/ml
644 heparin (Affymetrix), 10^{-6} M hydrocortisone (Sigma), 100ng/ml SCF (R & D Systems), 5
645 ng/ml IL-3 (R & D Systems), 3 IU/ml Epo (Amgen) and 5% plasma (Octapharma) at 37°C
646 in 5% CO2 in air, as previously described (Egan et al., 2015; Giarratana et al., 2011). On
647 the 2nd day of the culture, the cells were subjected to nucleofection with ribonucleoprotein
648 (RNP) complexes as described below. On day 5, the cells were washed and resuspended
649 in fresh cPIMDM to maintain concentration ~ $1x10^4$/ml. Between day 8-13, the cells were

650 maintained in fresh cPIMDM devoid of IL3 and hydrocortisone at concentration of <$5x10^5$
651 cells/ml. On day 13, the cells were washed and plated at $7.5x10^5$ - $1.0x10^6$cells/ml in
652 cPIMDM without IL-3, hydrocortisone, or SCF. On day 15-16, the cells were co-cultured
653 at $1.0x10^6$cells/ml concentration on a murine stromal cell layer (MS-5), as previously
654 described (Giarratana et al., 2005). The cells were harvested on days 18-22 for different
655 experiments. Growth and differentiation were monitored using hemocytometer-based
656 quantification and light microscopy of cytospin preparations stained with May-Grünwald
657 and Giemsa. To quantify the enucleation rate, cRBCs were incubated in Vybrant
658 DyeCycle violet (Life Technologies) (1:10,000) at 37°C for 30 min, followed by flow
659 cytometry analysis on a MACSQuant flow cytometer (Miltenyi).
660

661 **CRISPR-Cas9 genetic modification of primary human CD34+ cells**

662 Two sgRNAs targeting human *CD55* exons were designed using the Broad Institute's
663 GPP sgRNA design portal and synthesized as chemically modified sgRNAs by Synthego.
664 The sgRNA sequences were: GGGCCCCUACUCACCCCACA, which is predicted to
665 recognize a sequence in exon 1 of *CD55*, and CUGGGCAUUAGGUACAUCUG, which is
666 predicted to recognize a sequence in exon 2. Ribonucleoprotein (RNP) complexes
667 containing one or both sgRNAs were prepared by slowly adding 300 pmol of each sgRNA
668 to 150 pmol Cas9 protein in a 10 µl final volume with nuclease-free water and incubating
669 at room temperature for 10 min. On day 2 after thawing CD34+ cells, the RNP complexes
670 were added to $1X10^5$ cells in 40 µl of P3 nucleofection buffer from the 4D-Nucleofector X
671 kit (Lonza). Half of the mixture was loaded to each well of a 16-well nucleofection cassette
672 and nucleofected using the using E0-100 program with the 4D-Nucleofector Lonza

673 Amaxa. After nucleofection, cells were transferred to 6 ml fresh cPIMDM and incubated
674 at 37°C in 5% CO2 in air.
675
676 **Enrichment of CD71 negative cRBCs**
677 Fully differentiated cRBCs were washed in degassed and chilled bead buffer (PBS + 0.5%
678 bovine serum albumin + 2mM EDTA), resuspended in the same buffer (45 µl for $6x10^6$
679 cells), and incubated the anti-CD71 antibody-immoblized beads (Miltenyi) (10µl beads for
680 $6x10^6$ cells) at 4°C for 15 min. The cells were washed in 1 ml of bead buffer and passed
681 through an LS magnetic column (Miltenyi) and washed 3 times with 2 ml of the buffer.
682 The flow through containing CD71- negative cells was collected, washed with cRPMI
683 medium and used for invasion assays.
684
685 **Detection of cell surface proteins by flow cytometry**
686 Expression of RBC surface proteins was measured in control or knockout cRBCs by flow
687 cytometry. $1x10^6$ cRBCs were washed 2 times with PBS/0.3% BSA and incubated with
688 primary monoclonal antibodies or fluorochrome conjugated antibodies at 4°C for 1 h.
689 Antibodies used: anti-CD55 (BRIC 216-PE, IBGRL; 1:50) and anti-CD71-PE (Miltenyi;
690 1:20). After incubation, the cells were washed 2 times in PBS/0.3% BSA, followed by flow
691 cytometry analysis on a MACSQuant flow cytometer (Miltenyi).
692
693 **Immunofluorecence assays (IFA)**
694 IFAs were performed as previously described, with some modifications (Tonkin et al.,
695 2004). For IFAs of CD55-CRISPR cRBCs infected with *P. falciparum*, cells were fixed in

696 4.0% paraformaldehyde and 0.0015% glutaraldehyde in PBS for 20 min at room
697 temperature and blocked for one hour in 3% BSA/PBS. The cells were incubated with
698 anti-CD55 antibody (BRIC 216-PE from IBGRL) at 1:50 concentration for 1 h at 4°C. Cells
699 were mounted Fluoromount-G with DAPI mounting medium (Electron Microscopy
700 Services) and the fluorescent images were captured with a 60X objective on a Keyence
701 BZ-X700 fluorescence microscope. For IFAs of merozoites attached to pRBCs, samples
702 were prepared as in the attachment assays (see below), and 60 ul of the samples were
703 fixed in the fixative containing 4.0% Paraformaldehyde and 0.015% Glutaraldehyde for
704 20 min, washed twice in PBS, and allowed to settle onto a Poly-L-Lysine coated coverslip
705 (Corning). The samples were then incubated in 0.1% Triton X-100/PBS for 10 min at
706 room temperature, washed in PBS, and incubated in 0.1mg/ml of NaBH4/PBS for 10 min.
707 at room temperature. Following a wash in PBS, the cells were blocked overnight in fresh
708 PBS/3.0% BSA at room temperature. Primary antibodies: mouse monoclonal Anti-
709 PfAMA1 1F9 (1:200) (Coley et al., 2001) and rabbit polyclonal anti-PfRON4 (1:200)
710 (Richard et al., 2010) were diluted in blocking buffer applied to cells for 2 hr at room
711 temperature. Following 3 washes, the cells were incubated in corresponding secondary
712 antibodies at 1:500 dilution: Alexa Fluor 555 (anti-rabbit) and Alexa Fluor 488 (anti-
713 mouse) for 1 h at room temperature. The cells were washed in PBS supplemented with
714 0.1ng/µl of DAPI (Thermofisher) and mounted in Vectashield anti-fade mounting medium.
715 Imaging was performed using a Zeiss LSM710 confocal microscope and the image
716 analysis was performed using Fiji/imageJ (Version 2.0.0-rc-69/1.52i). Apical orientation
717 was defined as PfAMA1 and PfRON4 co-localization at the cellular interface, and non-
718 apical orientation was defined as PfAMA1 and PfRON4 not co-localized at the cellular

719 interface. Merozoites were defined as being mid-invasion if AMA1 and RON4 were co-
720 localized at cellular interface and the merozoite appeared to protrude into the RBC,
721 creating an indentation.
722
723 **Anti-CD55 polyclonal antibody generation**
724 A CD55 cDNA (Asp 35-Ser 353) was cloned into a modified pTT5 vector (Raymond et
725 al., 2011), whose expression cassette consists of eGFP fused to a puromycin resistance
726 gene followed by a 2A skip peptide (Funston, Kallioinen, de Felipe, Ryan, & Iggo, 2008)
727 and a BiP signal peptide, and the resulting plasmid was verified by sequencing. 1.8L of
728 293-6E cells grown in Freestyle 293 media (Invitrogen) to 0.8x10e6 cells/ml were
729 transfected with linear PEI (Polysciences) with 397ug DNA at a 1:3 DNA:PEI
730 ratio. TN1 tryptone (Organotechnie) was added to a final concentration of 0.5% (w/v)
731 one day after transfection, and cells were grown for an additional 5 days. Cells were spun
732 down and discarded, and the following reagents were added to the harvested media (final
733 concentration listed): 20mM Tris pH8, 350mM NaCl, 5mM Imidazole pH8, 0.2mM
734 NiCl2. 6ml GE IMAC sepharose 6 beads, and the sample was rocked at 4C for 1
735 hour. The sample was then poured into a glass column, and washed with 50ml of TBS
736 (10mM Tris pH8, 500mM NaCl) with imidazole at the following concentrations
737 sequentially: 5mM, 10mM, 50mM, and 250mM. Nickel was stripped from the column with
738 10ml 100mM EDTA. The majority of the CD55-8xHis protein eluted in the 250mM
739 Imidazole fraction, with a smaller amount of equal purity in the 50mM imadazole
740 fraction. These were dialyzed separately into PBS pH 7.4 overnight at 4C, concentrated
741 to 10mg/ml using Amicon Ultra 15 with 30kDa cutoff (Millipore), snap frozen in liquid

742 nitrogen and stored at -80C until further use. 2.5 mg of CD55-8xHis was used for three
743 immunizations of two New Zealand white-SPF rabbits by New England Peptide.
744 Approximately 50ml of recovered antiserum was used for negative affinity purification with
745 an 8X HIS column, and subsequently purified with a protein A column. Approximately 15
746 ml of purified IgG at 1.209 mg/ml concentration was purified and stored at -80C
747 until further use.
748
749
750 **Live cell imaging**
751 Schizont stage *P. falciparum* strain 3D7 parasites at 4-5% parasitemia and 2% hematocrit
752 were tightly synchronized with 2 μM Compound 2 to prevent schizont rupture (Collins et
753 al., 2013). After ~4-6 hour incubation, they were washed three times and allowed to
754 recover in fresh cRPMI for 45 to 90 minutes at 37º C. After recovery, anti-CD55 antibody
755 or IgG isotype control was added to the cells at final antibody concentration of 400 μg/ml
756 and 1% hematocrit. In experiments involving previously cryopreserved CD55-null pRBCs
757 (Takahashi, 2008) or control WT pRBCs, late stage *P. falciparum* schizonts were isolated
758 using a MACS magnet, synchronized with Compound 2, and then mixed with the pRBCs
759 at 4-5% parasitemia and 1% hematocrit. The assays were loaded into a 20 mm diameter
760 Hybriwell sealing system (Grace Bio-labs) customized for live cell imaging. Rupture of the
761 parasite-infected red blood cells and subsequent invasion events were video recorded
762 using a 60X objective Keyence BZ-X700 live microscopy setup at 37°C supplied with 5%
763 CO_2 and 1% O_2 gaseous environment. For the live cell imaging of echinocytosis, 1μM
764 Cytochalasin D was added to the above mixtures. Kinetics and morphology of distinct

765 steps of invasion in the video were measured by using ImageJ (ImageJ 1.50i) as
766 described previously(Schneider et al., 2012; Weiss et al., 2015). Briefly, the following
767 events were quantified in each video: a) Contacts between merozoites and RBCs that
768 culminated in successful invasion; b) successful invasion that resulted echinocytosis; c)
769 contacts between merozoites and RBCs that could not proceed beyond initial
770 contact/deformation. d) RBCs contacted before successful invasion e) period of pre-
771 invasion (initial contact to end of deformation), f) during of internalization, g) time to the
772 onset of echinocytosis, h) efficiency and degree of merozoite-induced deformation of the
773 target RBC using a four-point deformation scale (0,1,2,3).
774
775 **Merozoite attachment assays**
776 Purified schizonts were added at 12.0% parasitemia to previously cryopreserved CD55-
777 null pRBCs (Takahashi, 2008) or control WT pRBCs at 1.0% hematocrit in the presence
778 of 1 μM Cytochalasin D, 50 U/ml Heparin or none in a final volume of 100 ul per well in a
779 96 well plate. The mixtures were incubated at 37°C for 90 min and the schizonts were
780 allowed to rupture. To quantify merozoite attachment by flow cytometry, 10 μl aliquots of
781 the samples were fixed in 2% Glutaraldehyde and 0.116M sucrose in PBS, washed in
782 PBS/0.3% BSA, and stained with SYBR Green 1 nucleic acid stain (Invitrogen). at 1:2000
783 dilution in PBS/0.3% BSA for 20 minutes, followed by flow cytometry analysis on a
784 MACSQuant flow cytometer (Miltenyi). The assays were performed 3 times with 3
785 technical replicates. The merozoite attachment rates to control or CD55-null RBCs were
786 calculated as the percent of RBCs with an attached merozoite, and were normalized for
787 background attachment in the presence of heparin. The merozoite attachment efficiency

788 was calculated for each genetic background in each biological replicate by normalizing to

789 the mean of the attachment rates in the three control experiments.

790

791 **Data analysis**

792 Stastistical analyses were performed and the graphs were generated using GraphPad Prism

793 8 Version 8.0.2 (159) for macOS.

794
795

796 **Supplemental Information**
797 Supplemental information includes six figures and eight movies.

798

799 **Multimedia Files**

800 Movie S1: *P. falciparum* 3D7 invasion in the presence of isotype control antibody.

801 Movie S2: *P. falciparum* 3D7 invasion in the presence of anti-CD55 antibody.

802 Movie S3: *P. falciparum* 3D7 merozoite-induced deformation with deformation score 1.

803 Movie S4: *P. falciparum* 3D7 merozoite-induced deformation with deformation score 2.

804 Movie S5: *P. falciparum* 3D7 merozoite-induced deformation with deformation score 3.

805 Movie S6: An example of a failed invasion despite successful merozoite-induced
806 deformation in CD55-null pRBC.

807 Movie S7: An example of a successful invasion of a wild-type pRBC.

808 Movie S8: Echinocytosis induced by attached *P. falciparum* merozoite to pRBCs in the
809 presence of Cytochalasin D. Black arrows: Attachment resulting echinocyte formation.
810 White arrows: Attachment resulting no echinocyte formation.

811

812

813

References

Alexander, D. L., Arastu-Kapur, S., Dubremetz, J. F., & Boothroyd, J. C. (2006). *Plasmodium falciparum* AMA1 binds a rhoptry neck protein homologous to TgRON4, a component of the moving junction in *Toxoplasma gondii*. *Eukaryot Cell, 5*(7), 1169-1173. doi:10.1128/EC.00040-06

Alexander, D. L., Mital, J., Ward, G. E., Bradley, P., & Boothroyd, J. C. (2005). Identification of the moving junction complex of *Toxoplasma gondii*: a collaboration between distinct secretory organelles. *PLoS Pathog, 1*(2), e17. doi:10.1371/journal.ppat.0010017

Bei, A. K., & Duraisingh, M. T. (2012). Functional analysis of erythrocyte determinants of *Plasmodium infection*. *Int J Parasitol, 42*(6), 575-582. doi:10.1016/j.ijpara.2012.03.006

Besteiro, S., Dubremetz, J. F., & Lebrun, M. (2011). The moving junction of apicomplexan parasites: a key structure for invasion. *Cell Microbiol, 13*(6), 797-805. doi:10.1111/j.1462-5822.2011.01597.x

Besteiro, S., Michelin, A., Poncet, J., Dubremetz, J. F., & Lebrun, M. (2009). Export of a *Toxoplasma gondii* rhoptry neck protein complex at the host cell membrane to form the moving junction during invasion. *PLoS Pathog, 5*(2), e1000309. doi:10.1371/journal.ppat.1000309

Chen, L., Lopaticki, S., Riglar, D. T., Dekiwadia, C., Uboldi, A. D., Tham, W. H., . . . Cowman, A. F. (2011). An EGF-like protein forms a complex with PfRh5 and is required for invasion of human erythrocytes by *Plasmodium falciparum*. *PLoS Pathog, 7*(9), e1002199. doi:10.1371/journal.ppat.1002199

Chu, T. T. T., Sinha, A., Malleret, B., Suwanarusk, R., Park, J. E., Naidu, R., . . . Chandramohanadas, R. (2018). Quantitative mass spectrometry of human reticulocytes reveal proteome-wide modifications during maturation. *Br J Haematol, 180*(1), 118-133. doi:10.1111/bjh.14976

Coley, A. M., Campanale, N. V., Casey, J. L., Hodder, A. N., Crewther, P. E., Anders, R. F., . . . Foley, M. (2001). Rapid and precise epitope mapping of monoclonal antibodies against *Plasmodium falciparum* AMA1 by combined phage display of fragments and random peptides. *Protein Eng, 14*(9), 691-698. doi:10.1093/protein/14.9.691

Collins, C. R., Hackett, F., Strath, M., Penzo, M., Withers-Martinez, C., Baker, D. A., & Blackman, M. J. (2013). Malaria parasite cGMP-dependent protein kinase regulates blood stage merozoite secretory organelle discharge and egress. *PLoS Pathog, 9*(5), e1003344. doi:10.1371/journal.ppat.1003344

857 Cooling, L. (2015). Blood Groups in Infection and Host Susceptibility. *Clin Microbiol Rev, 28*(3),
858 801-870. doi:10.1128/CMR.00109-14
859
860 Coyne, C. B., & Bergelson, J. M. (2006). Virus-induced Abl and Fyn kinase signals permit
861 coxsackievirus entry through epithelial tight junctions. *Cell, 124*(1), 119-131.
862 doi:10.1016/j.cell.2005.10.035
863
864 Crosnier, C., Bustamante, L. Y., Bartholdson, S. J., Bei, A. K., Theron, M., Uchikawa, M., . . .
865 Wright, G. J. (2012). Basigin is a receptor essential for erythrocyte invasion by
866 *Plasmodium falciparum*. *Nature, 480*(7378), 534-537. doi:nature10606 [pii]
867 10.1038/nature10606
868
869 Dreyer, A. M., Matile, H., Papastogiannidis, P., Kamber, J., Favuzza, P., Voss, T. S., . . . Pluschke,
870 G. (2012). Passive immunoprotection of *Plasmodium falciparum*-infected mice
871 designates the CyRPA as candidate malaria vaccine antigen. *J Immunol, 188*(12), 6225-
872 6237. doi:10.4049/jimmunol.1103177
873
874 Dvorak, J. A., Miller, L. H., Whitehouse, W. C., & Shiroishi, T. (1975). Invasion of erythrocytes by
875 malaria merozoites. *Science, 187*(4178), 748-750. doi:10.1126/science.803712
876
877 Egan, E. S. (2017). Beyond Hemoglobin: Screening for Malaria Host Factors. *Trends Genet*.
878 doi:10.1016/j.tig.2017.11.004
879
880 Egan, E. S., Jiang, R. H., Moechtar, M. A., Barteneva, N. S., Weekes, M. P., Nobre, L. V., . . .
881 Duraisingh, M. T. (2015). Malaria. A forward genetic screen identifies erythrocyte CD55
882 as essential for *Plasmodium falciparum* invasion. *Science, 348*(6235), 711-714.
883 doi:10.1126/science.aaa3526
884
885 Funston, G. M., Kallioinen, S. E., de Felipe, P., Ryan, M. D., & Iggo, R. D. (2008). Expression of
886 heterologous genes in oncolytic adenoviruses using picornaviral 2A sequences that
887 trigger ribosome skipping. *J Gen Virol, 89*(Pt 2), 389-396. doi:10.1099/vir.0.83444-0
888
889 Gautier, E. F., Ducamp, S., Leduc, M., Salnot, V., Guillonneau, F., Dussiot, M., . . . Mayeux, P.
890 (2016). Comprehensive Proteomic Analysis of Human Erythropoiesis. *Cell Rep, 16*(5),
891 1470-1484. doi:10.1016/j.celrep.2016.06.085
892
893 Giarratana, M. C., Kobari, L., Lapillonne, H., Chalmers, D., Kiger, L., Cynober, T., . . . Douay, L.
894 (2005). Ex vivo generation of fully mature human red blood cells from hematopoietic
895 stem cells. *Nat Biotechnol, 23*(1), 69-74. doi:nbt1047 [pii]10.1038/nbt1047
896
897 Giarratana, M. C., Rouard, H., Dumont, A., Kiger, L., Safeukui, I., Le Pennec, P. Y., . . . Douay, L.
898 (2011). Proof of principle for transfusion of in vitro-generated red blood cells. *Blood,*
899 *118*(19), 5071-5079. doi:blood-2011-06-362038 [pii] 10.1182/blood-2011-06-362038
900

901 Gilson, P. R., & Crabb, B. S. (2009). Morphology and kinetics of the three distinct phases of red
902 blood cell invasion by *Plasmodium falciparum* merozoites. *Int J Parasitol, 39*(1), 91-96.
903 doi:10.1016/j.ijpara.2008.09.007
904
905 Harvey, K. L., Yap, A., Gilson, P. R., Cowman, A. F., & Crabb, B. S. (2014). Insights and
906 controversies into the role of the key apicomplexan invasion ligand, Apical Membrane
907 Antigen 1. *Int J Parasitol, 44*(12), 853-857. doi:10.1016/j.ijpara.2014.08.001
908
909 Hendel, A., Bak, R. O., Clark, J. T., Kennedy, A. B., Ryan, D. E., Roy, S., . . . Porteus, M. H. (2015).
910 Chemically modified guide RNAs enhance CRISPR-Cas genome editing in human primary
911 cells. *Nat Biotechnol, 33*(9), 985-989. doi:10.1038/nbt.3290
912
913 Hu, G., Cabrera, A., Kono, M., Mok, S., Chaal, B. K., Haase, S., . . . Bozdech, Z. Transcriptional
914 profiling of growth perturbations of the human malaria parasite *Plasmodium falciparum*.
915 *Nat Biotechnol, 28*(1), 91-98. doi:nbt.1597 [pii] 10.1038/nbt.1597
916
917 Hu, J., Liu, J., Xue, F., Halverson, G., Reid, M., Guo, A., . . . An, X. (2013). Isolation and functional
918 characterization of human erythroblasts at distinct stages: implications for
919 understanding of normal and disordered erythropoiesis in vivo. *Blood, 121*(16), 3246-
920 3253. doi:10.1182/blood-2013-01-476390
921
922 Kanjee, U., Gruring, C., Chaand, M., Lin, K. M., Egan, E., Manzo, J., . . . Duraisingh, M. T. (2017).
923 CRISPR/Cas9 knockouts reveal genetic interaction between strain-transcendent
924 erythrocyte determinants of *Plasmodium falciparum* invasion. *Proc Natl Acad Sci U S A,*
925 *114*(44), E9356-E9365. doi:10.1073/pnas.1711310114
926
927 Koch, M., & Baum, J. (2016). The mechanics of malaria parasite invasion of the human
928 erythrocyte - towards a reassessment of the host cell contribution. *Cell Microbiol, 18*(3),
929 319-329. doi:10.1111/cmi.12557
930
931 Malleret, B., Xu, F., Mohandas, N., Suwanarusk, R., Chu, C., Leite, J. A., . . . Russell, B. (2013).
932 Significant biochemical, biophysical and metabolic diversity in circulating human cord
933 blood reticulocytes. *PLoS One, 8*(10), e76062. doi:10.1371/journal.pone.0076062
934
935 Miller, L. H., Aikawa, M., Johnson, J. G., & Shiroishi, T. (1979). Interaction between cytochalasin
936 B-treated malarial parasites and erythrocytes. Attachment and junction formation. *J Exp*
937 *Med, 149*(1), 172-184.
938
939 Ord, R. L., Rodriguez, M., & Lobo, C. A. (2015). Malaria invasion ligand RH5 and its prime
940 candidacy in blood-stage malaria vaccine design. *Hum Vaccin Immunother, 11*(6), 1465-
941 1473. doi:10.1080/21645515.2015.1026496
942

943 Pasvol, G., Chasis, J. A., Mohandas, N., Anstee, D. J., Tanner, M. J., & Merry, A. H. (1989).
944 Inhibition of malarial parasite invasion by monoclonal antibodies against glycophorin A
945 correlates with reduction in red cell membrane deformability. *Blood, 74*(5), 1836-1843.
946
947 Paul, A. S., Egan, E. S., & Duraisingh, M. T. (2015). Host-parasite interactions that guide red
948 blood cell invasion by malaria parasites. *Curr Opin Hematol, 22*(3), 220-226.
949 doi:10.1097/MOH.0000000000000135
950
951 Raymond, C., Tom, R., Perret, S., Moussouami, P., L'Abbe, D., St-Laurent, G., & Durocher, Y.
952 (2011). A simplified polyethylenimine-mediated transfection process for large-scale and
953 high-throughput applications. *Methods, 55*(1), 44-51. doi:10.1016/j.ymeth.2011.04.002
954
955 Reddy, K. S., Amlabu, E., Pandey, A. K., Mitra, P., Chauhan, V. S., & Gaur, D. (2015). Multiprotein
956 complex between the GPI-anchored CyRPA with PfRH5 and PfRipr is crucial for
957 *Plasmodium falciparum* erythrocyte invasion. *Proc Natl Acad Sci U S A, 112*(4), 1179-
958 1184. doi:10.1073/pnas.1415466112
959
960 Richard, D., MacRaild, C. A., Riglar, D. T., Chan, J. A., Foley, M., Baum, J., . . . Cowman, A. F.
961 (2010). Interaction between *Plasmodium falciparum* apical membrane antigen 1 and the
962 rhoptry neck protein complex defines a key step in the erythrocyte invasion process of
963 malaria parasites. *J Biol Chem, 285*(19), 14815-14822. doi:10.1074/jbc.M109.080770
964
965 Riglar, D. T., Richard, D., Wilson, D. W., Boyle, M. J., Dekiwadia, C., Turnbull, L., . . . Baum, J.
966 (2011). Super-resolution dissection of coordinated events during malaria parasite
967 invasion of the human erythrocyte. *Cell Host Microbe, 9*(1), 9-20.
968 doi:10.1016/j.chom.2010.12.003
969
970 Sack, B., Kappe, S. H., & Sather, D. N. (2017). Towards functional antibody-based vaccines to
971 prevent pre-erythrocytic malaria infection. *Expert Rev Vaccines, 16*(5), 403-414.
972 doi:10.1080/14760584.2017.1295853
973
974 Salinas, N. D., Tang, W. K., & Tolia, N. H. (2019). Blood-Stage Malaria Parasite Antigens:
975 Structure, Function, and Vaccine Potential. *J Mol Biol, 431*(21), 4259-4280.
976 doi:10.1016/j.jmb.2019.05.018
977
978 Satchwell, T. J., Wright, K. E., Haydn-Smith, K. L., Sanchez-Roman Teran, F., Moura, P. L.,
979 Hawksworth, J., . . . Baum, J. (2019). Genetic manipulation of cell line derived
980 reticulocytes enables dissection of host malaria invasion requirements. *Nat Commun,*
981 *10*(1), 3806. doi:10.1038/s41467-019-11790-w
982
983 Schneider, C. A., Rasband, W. S., & Eliceiri, K. W. (2012). NIH Image to ImageJ: 25 years of Image
984 Analysis. *Nature Methods, 9*(7), 671-675.
985

986 Scully, E. J., Shabani, E., Rangel, G. W., Gruring, C., Kanjee, U., Clark, M. A., . . . Duraisingh, M. T.
987 (2019). Generation of an immortalized erythroid progenitor cell line from peripheral
988 blood: A model system for the functional analysis of *Plasmodium* spp. invasion. *Am J*
989 *Hematol, 94*(9), 963-974. doi:10.1002/ajh.25543
990
991 Spadafora, C., Awandare, G. A., Kopydlowski, K. M., Czege, J., Moch, J. K., Finberg, R. W., . . .
992 Stoute, J. A. (2010). Complement receptor 1 is a sialic acid-independent erythrocyte
993 receptor of *Plasmodium falciparum*. *PLoS Pathog, 6*(6), e1000968.
994 doi:10.1371/journal.ppat.1000968
995
996 Srinivasan, P., Beatty, W. L., Diouf, A., Herrera, R., Ambroggio, X., Moch, J. K., . . . Miller, L. H.
997 (2011). Binding of *Plasmodium* merozoite proteins RON2 and AMA1 triggers
998 commitment to invasion. *Proc Natl Acad Sci U S A, 108*(32), 13275-13280.
999 doi:10.1073/pnas.1110303108
1000
1001 Storry, J. R., Reid, M. E., & Yazer, M. H. (2010). The Cromer blood group system: a review.
1002 *Immunohematology, 26*(3), 109-118.
1003
1004 Takahashi, J. Y. S., Yamane S, Tanaka M, Takahashi H, et al. (2008). A case of Inab phenotype
1005 (IFC-) with anti-IFC. *Jpn J Transfusion and Cell Therapy, 54*(2), 258.
1006
1007 Taylor, S. M., & Fairhurst, R. M. (2014). Malaria parasites and red cell variants: when a house is
1008 not a home. *Curr Opin Hematol, 21*(3), 193-200. doi:10.1097/MOH.0000000000000039
1009
1010 Tham, W. H., Healer, J., & Cowman, A. F. (2012). Erythrocyte and reticulocyte binding-like
1011 proteins of *Plasmodium falciparum*. *Trends Parasitol, 28*(1), 23-30.
1012 doi:10.1016/j.pt.2011.10.002
1013
1014 Tiffert, T., Lew, V. L., Ginsburg, H., Krugliak, M., Croisille, L., & Mohandas, N. (2005). The
1015 hydration state of human red blood cells and their susceptibility to invasion by
1016 *Plasmodium falciparum*. *Blood, 105*(12), 4853-4860. doi:10.1182/blood-2004-12-4948
1017
1018 Tonkin, C. J., van Dooren, G. G., Spurck, T. P., Struck, N. S., Good, R. T., Handman, E., . . .
1019 McFadden, G. I. (2004). Localization of organellar proteins in Plasmodium falciparum
1020 using a novel set of transfection vectors and a new immunofluorescence fixation
1021 method. *Mol Biochem Parasitol, 137*(1), 13-21. doi:10.1016/j.molbiopara.2004.05.009
1022
1023 Volz, J. C., Yap, A., Sisquella, X., Thompson, J. K., Lim, N. T., Whitehead, L. W., . . . Cowman, A. F.
1024 (2016). Essential Role of the PfRh5/PfRipr/CyRPA Complex during *Plasmodium*
1025 *falciparum* Invasion of Erythrocytes. *Cell Host Microbe, 20*(1), 60-71.
1026 doi:10.1016/j.chom.2016.06.004
1027
1028 Weiss, G. E., Gilson, P. R., Taechalertpaisarn, T., Tham, W. H., de Jong, N. W., Harvey, K. L., . . .
1029 Crabb, B. S. (2015). Revealing the Sequence and Resulting Cellular Morphology of

1030 Receptor-Ligand Interactions during *Plasmodium falciparum* Invasion of Erythrocytes.
1031 *PLoS Pathog, 11*(2), e1004670. doi:10.1371/journal.ppat.1004670
1032
1033 WHO. (2018). *World Malaria Report 2018*. World Health Organization, Geneva.
1034
1035 Yap, A., Azevedo, M. F., Gilson, P. R., Weiss, G. E., O'Neill, M. T., Wilson, D. W., . . . Cowman, A.
1036 F. (2014). Conditional expression of apical membrane antigen 1 in *Plasmodium*
1037 *falciparum* shows it is required for erythrocyte invasion by merozoites. *Cell Microbiol,*
1038 *16*(5), 642-656. doi:10.1111/cmi.12287
1039